

# Stochastic dynamics and mechanosensitivity of myosin II minifilaments

Philipp J. Albert, Thorsten Erdmann, and Ulrich S. Schwarz\*

*BioQuant, Heidelberg University, Im Neuenheimer Feld 267,  
69120 Heidelberg, Germany and Institute for Theoretical Physics,  
Heidelberg University, Philosophenweg 19, 69120 Heidelberg, Germany*

(Dated: June 27, 2021)

## Abstract

Tissue cells are in a state of permanent mechanical tension that is maintained mainly by myosin II minifilaments, which are bipolar assemblies of tens of myosin II molecular motors contracting actin networks and bundles. Here we introduce a stochastic model for myosin II minifilaments as two small myosin II motor ensembles engaging in a stochastic tug-of-war. Each of the two ensembles is described by the parallel cluster model that allows us to use exact stochastic simulations and at the same time to keep important molecular details of the myosin II cross-bridge cycle. Our simulation and analytical results reveal a strong dependence of myosin II minifilament dynamics on environmental stiffness that is reminiscent of the cellular response to substrate stiffness. For small stiffness, minifilaments form transient crosslinks exerting short spikes of force with negligible mean. For large stiffness, minifilaments form near permanent crosslinks exerting a mean force which hardly depends on environmental elasticity. This functional switch arises because dissociation after the power stroke is suppressed by force (catch bonding) and because ensembles can no longer perform the power stroke at large forces. Symmetric myosin II minifilaments perform a random walk with an effective diffusion constant which decreases with increasing ensemble size, as demonstrated for rigid substrates with an analytical treatment.

\*Correspondence: Ulrich.Schwarz@bioquant.uni-heidelberg.de

## I. INTRODUCTION

Cytoskeletal molecular motors are a large class of proteins that generate movement and force in biological cells by cycling between states bound and unbound from a cytoskeletal filament [1, 2]. In general, they can be classified as processive or non-processive motors. Processive motors like kinesin, dynein or myosin V have a duty ratio (fraction of time of the motor cycle spent on the filament) close to unity and therefore are particularly suited for persistent transport of cellular cargo, such as vesicles, small organelles or viruses. Using small groups of processive motors increases the walk length and the efficiency of transport compared to the single motor [3]. A theoretical treatment with a one-step master equation showed that the effective unbinding rate decreases exponentially with the size of the motor ensemble [4]. Moreover groups of motors can also work against larger load than the single motor [5]. If motors of different directionality on the substrate are attached to the same cargo, bidirectional movement can ensue [6], as often observed in cargo transport. A similar tug-of-war setup has been used earlier to explain mitotic spindle oscillations [7]. Non-processive motors such as myosin II have a duty ratio significantly smaller than unity. Therefore, non-processive motors have to operate in groups in order to generate appreciable levels of force. Similar to processive motors, the duty ratio of a group of non-processive motors increases with the size of the group and can become large enough that the group effectively behaves like a processive motor. This is certainly true for the sarcomeres in skeletal muscle, where typically hundreds of myosin II work together as one group. Combining structural investigations of skeletal muscle with modeling has led to the swinging cross-bridge model for single myosin II [8, 9]. A statistical treatment then has allowed to accurately model the dynamics of the motor ensemble in muscle sarcomeres [10, 11].

Groups of myosin II motors also play a crucial role for the mechanics and adhesion of non-muscle tissue cells. Cytoskeletal myosin II assembles into bipolar minifilaments consisting of 10-30 motors [12]. They interact with an actin cytoskeleton which is much less ordered than in muscle, mainly in the actin cortex as well as in the contractile actin networks and bundles associated with cell adhesion and migration [13]. Recently it has been shown that the activity of myosin II minifilaments contributes to the sorting of actin filament orientation because of the asymmetric elasticity of actin filaments [14, 15]. The myosin II based forces generated in the actin cytoskeleton are transmitted to the extracellular environment via adhesion sites, which have been shown to harbor different mechanosensitive processes [16, 17]. In particular, mature focal adhesions are

often connected to actin stress fibers consisting of parallel bundles of actin filaments with alternating polarity enabling myosin II minifilaments to contract the bundles and thus mechanically load the adhesion sites. To apply these forces effectively, the extracellular matrix underlying the adhesion sites must not be too soft. Therefore, cells are sensitive to the elasticity of the substrate and adhere preferentially to stiffer substrates [18]. If the environment is much stiffer than the cell, it essentially deforms itself and becomes insensitive to the environmental stiffness [19]. Therefore cellular stiffness sets the scale for the sensitivity of rigidity sensing [20]. Due to the complex interplay of many components in a cell, it is difficult to identify the exact contribution of myosin II to the rigidity response of cells. One promising experimental route is the reconstruction of *in vitro* systems of motors and filaments [15, 21–27], which in the future might allow us to probe these relations in more quantitative detail.

With the focus on the description of large assemblies of myosin II motors in the muscle sarcomere, theoretical progress has been made mainly through mean-field models [8, 28, 29] or computer simulations [10, 30, 31]. For ensembles consisting of a large number of motors, details about internal motor states are less important and experimentally accessible. Instead, collective quantities such as velocity, walk length and number of bound motor are of large interest. For example, generic two-state ratchet models have been used to study the behavior of mechanically coupled motors [32–34]. Here we aim at understanding minifilaments with few myosin II molecules for which molecular details and stochastic effects are expected to be more important. In this context, cross-bridge models are appropriate, which have been studied before mainly with computer simulations [10, 30, 35]. However, this approach is numerically costly, in particular for extensions to systems with multiple minifilaments. Recently the parallel cluster model (PCM) based on the cross-bridge cycle has been introduced as an efficient yet detailed model for stochastic effects in small myosin II ensembles [36, 37].

In this manuscript, we extend the PCM to myosin II minifilaments by modeling them as two ensembles of myosin II motors working against each other by walking along two actin tracks with opposing polarity. This situation can be considered as a tug-of-war of the two ensembles of non-processive motors, in analogy to a tug-of-war of processive motors [6, 7]. In contrast to those studies, however, we do not use a phenomenological force-velocity relation, but rather a cross-bridge model to explicitly include the molecular details of the motor cycle of myosin II. In particular, we account for the catch bond character of myosin II unbinding (dissociation rate decreases under load, in contrast to the classical case of a slip bond) and for the detailed kinetics

of the power stroke. From our model definition, it becomes clear that the mechanical situation in bipolar myosin II minifilaments is very complex, with an effective spring constant that depends on internal mechanics, external mechanics and the exact state of the motor ensembles. Our main result is that myosin II minifilaments show a kind of mechanosensitivity that is reminiscent of the way cells respond to environmental stiffness. We show that this effect not only results from the molecular catch-bonding property, but also from the inability to perform the power stroke in a stiff environment with sufficiently large force. We also find that catch-bonding of myosin II on stiff substrates leads to frequent switches of direction of the ensemble movement and therefore to an effective diffusion constant which decreases with increasing ensemble size, in marked contrast to a tug-of-war of processive motors with slip bonds.

## II. MODEL

In the parallel cluster model (PCM), individual myosin II motors are described by a cross-bridge model with three discrete states and stochastic transitions between them [36, 37]. Here we generalize this model for myosin II minifilaments and discuss it with parameter values originally introduced for modeling skeletal muscle [11, 30]. For cytoskeletal myosin II, these values depend on the exact isoform one is considering. The parameter values used here result in a duty ratio of 0.33, which lies in the range of duty ratios reported for cytoskeletal myosin II B [38, 39]. As shown schematically in Fig. 1 (a), a motor comprises three mechanical elements. The motor head binds to the substrate and contains the ATP hydrolysis site, which binds ATP or its hydrolysis products ADP and  $P_i$ . The rigid lever arm is hinged to the motor head and alternates between stretched and primed conformation, thus amplifying conformational changes in the motor head. The linear elastic neck linker with spring constant  $k_m = 2.5\text{pNnm}^{-1}$  anchors the lever arm to the rigid motor filament. In the unbound (*ub*) state, the motor head is loaded with ADP and  $P_i$  and the lever arm is primed. The motor reversibly transitions to the weakly-bound (*wb*) state with on-rate  $k_{01} \simeq 40\text{s}^{-1}$  and off-rate  $k_{10} \simeq 2\text{s}^{-1}$ . With release of  $P_i$ , the lever arm swings to the stretched conformation and the motor enters the post-power-stroke (*pps*) state. The power stroke is reversible with forward rate  $k_{12} \simeq 10^3\text{s}^{-1}$  and reverse rate  $k_{21} \simeq k_{12}$  but is driven towards the *pps* state by the free energy bias  $E_{pp} \simeq -60\text{pNnm}$ . This energy is stored in the primed conformation of the lever arm as part of the energy released in ATP hydrolysis. Replacing ADP by ATP, unbinding and ATP hydrolysis brings myosin II from the *pps* to the *ub* state, thus completing the motor cycle. These events are

subsumed in a single reaction with unloaded rate  $k_{20}^0 \simeq 80\text{s}^{-1}$  which is assumed to be irreversible due of the hydrolysis of ATP. Myosin II dynamics is characterized by the load dependence of power stroke and unbinding from *pps* state: the power stroke moves the lever arm by the power-stroke length  $d \simeq 8\text{nm}$ ; unbinding from the *pps* state requires an additional movement of the lever arm by a distance  $\delta \simeq 0.3\text{nm}$ . Thus, both reactions become slower under load. The reduced rate of unbinding under load makes the *pps* state of myosin II a catch bond rather than a slip bond in the range of forces considered here.

The arrangement of myosin II motors in a bipolar minifilament is depicted schematically in Fig. 1 (b). The minifilament consists of two ensembles of motors working in opposite direction. The motors are anchored to the rigid motor filament joining the two ensembles. Within each ensemble, motors are arranged in parallel whereas the two ensembles operate in series. The total number of motors in the ensemble working in (+) direction (towards the right in Fig. 1 (b)) is denoted by  $N_+$ ; the number of motors in the ensemble working in (−) direction (towards the left in Fig. 1 (b)) is denoted by  $N_-$ . The ensembles move on actin filaments of opposite polarity which are attached to linear elastic elements with spring constant  $K_+$  and  $K_-$  to represent the effective elasticity of the environment. The opposite polarity allows the minifilament to slide the actin filaments relative to each other and thereby to stretch the springs. The first approximation of the PCM is to assume that motors in equivalent mechano-chemical states exert equal forces (equal load sharing). This mean-field approximation is justified by the small duty ratio of non-processive motors. The elongation or strain of *wb* motors in (+) and (−) ensemble is denoted by  $x_+$  and  $x_-$ , respectively, so that *wb* motors exert the force  $k_m x_{\pm}$ . The strain is positive, when the neck linker is stretched against the moving direction of the ensemble (inwards in Fig. 1 (b)). With the assumption of equal load sharing, motor ensembles are mechanically equivalent to adhesion clusters of parallel bonds as depicted in Fig. 1 (c) [40]. In contrast to the adhesion cluster, however, the rest length of the bond is not fixed, but is reduced by a length  $d$  due to the power stroke. Thus, motors in the *pps* state have the strain  $x_{\pm} + d$  and exert the force  $k_m(x_{\pm} + d)$ . The strain of *wb* as well as *pps* motors is determined by the offset  $x_{\pm}$  between the bound motor head on the substrate and the anchor in the motor filament. The state  $(i_+, j_+; i_-, j_-)$  of a minifilament is described by the numbers  $i_+ \leq N_+$  and  $i_- \leq N_-$  of bound motors and  $j_+ \leq i_+$  and  $j_- \leq i_-$  of *pps* motors in both ensembles. The number of *ub* motors is  $N_{\pm} - i_{\pm}$  and that of *wb* motors  $i_{\pm} - j_{\pm}$ . With  $j_{\pm}$  *pps* motors and  $i_{\pm} - j_{\pm}$  *wb* motors, the ( $\pm$ ) ensemble exerts the force  $F_{\pm} = k_m [(i_{\pm} - j_{\pm})x_{\pm} + j_{\pm}(x_{\pm} + d)]$ . To determine the offset of *wb* and *pps* motors, we assume that a minifilament is always in mechanical

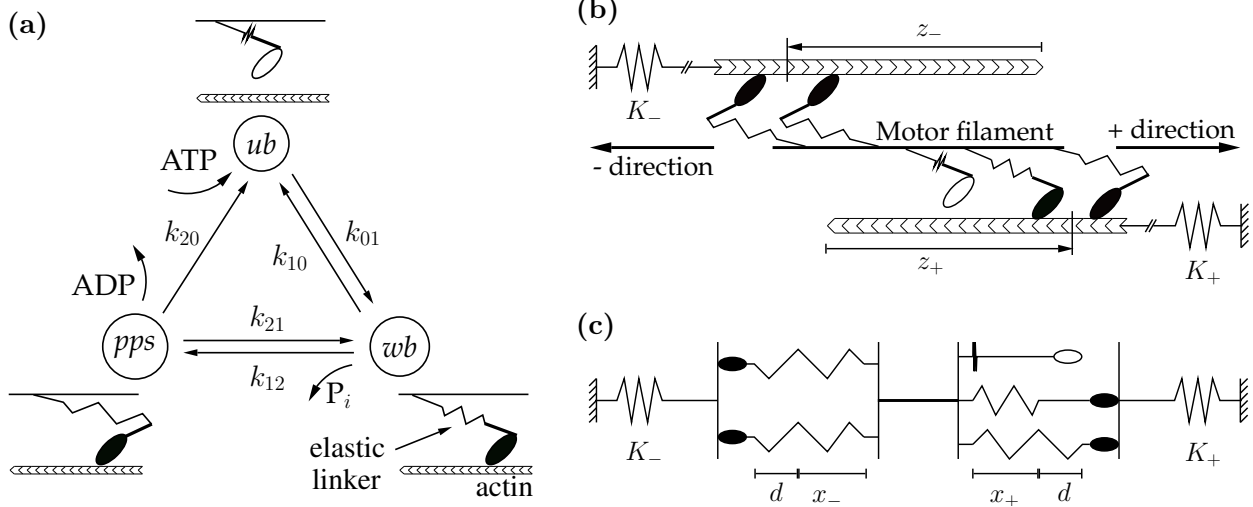


Figure 1. (a) Mechanical setup and hydrolysis cycle of myosin II. In the unbound (*ub*) state, the lever arm is primed and the neck linker has vanishing strain. In the weakly-bound (*wb*) state the motor head is bound to actin. The lever arm is primed but the neck linker generally has non-zero strain. In the post-power-stroke (*pps*) state the lever arm is stretched. Unbinding from *pps* state is the only irreversible transition because of the hydrolysis of ATP. (b) Bipolar minifilament with  $N_+ = 3$  motors in the (+) ensemble moving to the right and  $N_- = 2$  motors in the (-) ensemble moving to the left. The state of the ( $\pm$ ) ensemble is described by the number  $i_{\pm}$  of bound motors and the number  $j_{\pm}$  of motors in the post-power-stroke state. The configuration in (b) corresponds to  $(i_+, j_+) = (2, 1)$  in the (+) ensemble and  $(i_-, j_-) = (2, 2)$  in the (-) ensemble. The displacement of the ensembles on the actin filaments is denoted by  $z_+$  and  $z_-$ . Bound motors within each ensemble are arranged in parallel; the two ensembles are arranged in series. (c) The parallel cluster model (PCM) applied to a bipolar minifilament treats the motor ensembles as two adhesions clusters of parallel bonds coupled in series with external springs. All bound motors in equivalent mechano-chemical states have the same strain. The strain of weakly-bound (*wb*) motors is denoted by  $x_+$  and  $x_-$ . The power stroke shortens the rest length of the neck linker by the power-stroke length  $d$  so that post-power-stroke (*pps*) motors have the strain  $x_{\pm} + d$ .

equilibrium. For the arrangement of motor ensembles and external springs in series as in Fig. 1 (c) this requires that the ensemble forces  $F_{\pm}$  balance the force  $F_{\text{ext}}$  exerted by the external springs. The latter is  $F_{\text{ext}} = K_{\text{ext}} [z_+ + z_- - (x_+ + x_-)]$  where  $K_{\text{ext}} = K_+ K_- / (K_+ + K_-)$  is the effective external spring constant and  $z_{\pm}$  the displacement of the ( $\pm$ ) ensemble from its origin on the actin filament. The extension of the external springs is  $z_+ + z_- - (x_+ + x_-)$  assuming they are relaxed

when  $z_+ + z_- = 0$  and all bound motors are in the  $wb$  state with  $x_+ = x_- = 0$ . Solving the balance of forces,  $F_{\pm} = F_{\text{ext}}$ , yields  $x_{\pm}$  as function of minifilament state  $(i_+, j_+; i_-, j_-)$  and contraction  $z := z_+ + z_-$ ,

$$x_{\pm} = \frac{K_{\text{ext}}(zi_{\mp} + dj_{\mp}) - (K_{\text{ext}} + k_m i_{\mp})dj_{\pm}}{K_{\text{ext}}(i_{\pm} + i_{\mp}) + k_m i_{\pm} i_{\mp}}. \quad (1)$$

The force  $F_{\text{ext}} = F_{\pm}$  as function of minifilament state and contraction then reads

$$F_{\text{ext}} = K_{\text{tot}} \left[ z + d \left( \frac{j_+}{i_+} + \frac{j_-}{i_-} \right) \right], \quad (2)$$

where the total spring constant is defined as

$$K_{\text{tot}} = \frac{K_{\text{ext}} k_m i_+ i_-}{K_{\text{ext}}(i_+ + i_-) + k_m i_+ i_-} \quad (3)$$

and therefore varies dynamically, in contrast to  $K_{\text{ext}}$ . When all bound motors in the (+) ensemble are in the  $wb$  state ( $j_+ = 0$ ), the offset is positive,  $x_+ > 0$ , and the neck linkers are stretched against the (+) direction. For growing contraction  $z \geq 0$ , the offset  $x_+$  increases because  $F_{\text{ext}}$  increases. A growing number  $j_-$  of  $pps$  motors in the (-) ensemble increases  $x_+$  further, because transitions to the  $pps$  state shorten the minifilament and increase  $F_{\text{ext}}$ . On the other hand,  $x_+$  decreases and can become negative for a growing number  $j_+$  of  $pps$  motors in the (+) ensemble, although  $F_{\text{ext}}$  increases further. For  $x_+ < 0$ ,  $wb$  motors contribute to the external load which is carried by the  $pps$  motors whose strain is always positive,  $x_+ + d > 0$ .

The assumption of equal load sharing of equivalent motors defines a four dimensional network of minifilament states  $(i_+, j_+; i_-, j_-)$ . The second approximation of the PCM reduces this network further by assuming that bound states are in local thermal equilibrium (LTE). This is justified by the strong separation of time scales between fast power-stroke and slow binding kinetics [11, 36, 37]. In LTE, the conditional probability that  $(j_+, j_-)$  motors are in the  $pps$  state when  $(i_+, i_-)$  motors are bound is the Boltzmann distribution

$$p(i_+, i_- | j_+, j_-) = \exp(-E/k_B T) / Z_{i_+, i_-}, \quad (4)$$

where  $Z_{i_+, i_-} = \sum_{j_+=0}^{i_+} \sum_{j_-=0}^{i_-} \exp(-E/k_B T)$  is the partition sum. The energy  $E = E_{\text{ext}} + E_{\text{el},+} + E_{\text{el},-} + (j_+ + j_-)E_{\text{pp}}$  of a minifilament is the sum of the elastic energy in the external springs,  $E_{\text{ext}} = K_{\text{ext}} [z - (x_+ + x_-)]^2 / 2$ , the elastic energy  $E_{\text{el},+} + E_{\text{el},-}$  in the neck linkers, where  $E_{\text{el},\pm} = k_m [(i_{\pm} - j_{\pm})x_{\pm}^2 + j_{\pm}(x_{\pm} + d)^2] / 2$ , and the free energy bias  $E_{\text{pp}} < 0$  towards the  $pps$  state. Inserting Eq. (1) for  $x_{\pm}$  yields  $E$  as function of minifilament state  $(i_+, j_+; i_-, j_-)$  and

contraction  $z$ ,

$$E = \frac{K_{\text{tot}}}{2} \left[ z + d \left( \frac{j_+}{i_+} + \frac{j_-}{i_-} \right) \right]^2 + \frac{k_m d^2}{2} \left[ \frac{j_+ (i_+ - j_+)}{i_+} + \frac{j_- (i_- - j_-)}{i_-} \right] + (j_+ + j_-) E_{\text{pp}}. \quad (5)$$

The elastic energy is split into two contributions: the first is due to overall stretching of external springs and neck linkers. For  $z \geq 0$ , it increases with increasing contraction and number of bound motors in *pps* state. The second contribution is due to internal tension caused by motors in different bound states. It vanishes when all bound motors in an ensemble are either in *wb* state or in *pps* state, that is, for  $j_{\pm} = 0$  or  $j_{\pm} = i_{\pm}$ , and is positive for intermediate states with  $0 < j_{\pm} < i_{\pm}$ .

The LTE assumption for the bound states leaves the numbers  $i_+$  and  $i_-$  of bound motors as the only remaining variables. Binding and unbinding changes the state  $(i_+, i_-)$  by  $i_+ \rightarrow i_+ \pm 1$  and  $i_- \rightarrow i_- \pm 1$ . Binding proceeds only to the *wb* state and with constant on-rate  $k_{01} = \text{const}$ . Because  $N_{\pm} - i_{\pm}$  motors can bind independently the effective forward rate for the transition  $i_{\pm} \rightarrow i_{\pm} + 1$  in the  $(\pm)$  ensemble is

$$g_{\pm}(i_{\pm}) = (N_{\pm} - i_{\pm}) k_{01}. \quad (6)$$

The forward rate is independent of  $j_{\pm}$  and depends only on  $i_{\pm}$  in the respective ensemble. Unbinding of motors proceeds either with constant off-rate  $k_{10} = \text{const}$  from the *wb* state or with load dependent off-rate  $k_{20}(i_+, j_+; i_-, j_-)$  from the *pps* state. Thus, the reverse rate for the transition  $i_{\pm} \rightarrow i_{\pm} - 1$  in state  $(i_+, j_+; i_-, j_-)$  is

$$r_{\pm}(i_+, j_+; i_-, j_-) = (i_{\pm} - j_{\pm}) k_{10} + j_{\pm} k_{20}(i_+, j_+; i_-, j_-). \quad (7)$$

The effective reverse rate for transitions in state  $(i_+, i_-)$  is obtained by averaging over  $j_{\pm}$  with the LTE distribution from Eq. (4),

$$r_{\pm}(i_+, i_-) = \sum_{j_+=0}^{i_+} \sum_{j_-=0}^{i_-} r_{\pm}(i_+, j_+; i_-, j_-) p(j_+, j_- | i_+, i_-). \quad (8)$$

We use a Kramers type load dependence for the off-rate from the *pps* state,  $k_{20}(i_+, j_+; i_-, j_-) = k_{20}^0 \exp(-k_m(x_{\pm} + d)/F_0)$ . The off-rate decreases exponentially with increasing load  $k_m(x_{\pm} + d)$  on a motor to describe the catch bond character of the *pps* state, where  $F_0 = k_B T / \delta \simeq 12.6 \text{pN}$  sets the unbinding force scale. Inserting effective forward and reverse rate, a two dimensional master equation for the probability  $p_{i_+, i_-}(t)$  that  $(i_+, i_-)$  motors are bound can be formulated as

$$\begin{aligned} \frac{d}{dt} p_{i_+, i_-} &= r_+(i_+ + 1, i_-) p_{i_++1, i_-} + g_+(i_+ - 1) p_{i_+-1, i_-} \\ &+ r_-(i_+, i_- + 1) p_{i_+, i_-+1} + g_-(i_- - 1) p_{i_+, i_- - 1} \\ &- [r_+(i_+, i_-) + r_-(i_+, i_-) + g_+(i_+) + g_-(i_-)] p_{i_+, i_-}. \end{aligned} \quad (9)$$



The probability for a specific state  $(i_+, j_+; i_-, j_-)$  is the product of the coarse-grained probability distribution  $p_{i_+, i_-}(t)$  with the conditional LTE probability distribution  $p(j_+, j_- | i_+, i_-)$ . The master equation cannot be separated in two one-dimensional equations because the reverse rates  $r_+(i_+, i_-)$  and  $r_-(i_+, i_-)$  depend on  $i_+$  and  $i_-$  in both ensembles.

Because the effective reverse rates  $r_{\pm}(i_+, i_-)$  depend on the contraction  $z$ , the master equation for binding dynamics has to be solved together with rules for the displacement of the ensembles upon binding and unbinding [37]. We define the position  $z_{\pm}$  of an ensemble as the average position of bound motor heads on the substrate. The position of the motor filament is then given by  $z_{\pm} - x_{\pm}$ , where  $x_{\pm}$  is the offset of the motors. New motors are assumed to bind with vanishing offset, thus shifting the ensemble position by  $\Delta z_{\pm} = -x_{\pm}/(i_{\pm} + 1)$ . Note that the offset  $x_{\pm}$  is negative for ensembles subjected to small forces and with the majority of motors in the *pps* state. To implement the rules for ensemble movement with Eq. (9) the offset needs to be averaged with the LTE distribution. This gives  $\bar{x}_{\pm} = \sum_{j_+=0}^{i_+} \sum_{j_-=0}^{i_-} x_{\pm} p(j_+, j_- | i_+, i_-)$  in state  $(i_+, i_-)$  and the position change  $\Delta \bar{z}_{\pm} = -\bar{x}_{\pm}/(i_{\pm} + 1)$  upon binding of a motor. Unbinding of a motor does not change ensemble position because all bound motors are assumed to be at the same position  $z_{\pm}$ . Complete detachment of one ensemble relaxes the external springs and the still attached ensemble moves freely with offset  $x_{\mp} = -d$ . Reattachment therefore places the ensemble at  $z_{\pm} = z_{\mp} + x_{\mp}$ . Because  $z_+$  and  $z_-$  are defined in opposite directions, the sum  $z = z_+ + z_-$  describes the contraction of the actin substrates. With these definitions, the PCM for myosin II minifilaments is completely defined.

### III. RESULTS

#### A. Transitions in the power-stroke probability

The LTE distribution  $p(j_+, j_- | i_+, i_-)$  is shaped by the three parts of the minifilament energy  $E$  in Eq. (5). The second part—elastic energy due to internal tension of opposing motors in both ensembles—is symmetric against exchanging  $j_{\pm}$  and  $i_{\pm} - j_{\pm}$ . It vanishes when all bound motors are either in *pps* state ( $j_{\pm} = i_{\pm}$ ) or in *wb* state ( $j_{\pm} = 0$ ). Between  $j_{\pm} = 0$  and  $j_{\pm} = 1$  (or  $j_{\pm} = i_{\pm}$  to  $j_{\pm} = i_{\pm} - 1$ ) the energy increases by  $\Delta E \geq k_m d^2/4 \simeq 40 \text{pNnm}^{-1} \simeq 10 k_B T$  so that the relative occupancy is  $e^{-\Delta E/k_B T} \leq 10^{-4}$ . This implies that intermediate states with  $0 < j_{\pm} < i_{\pm}$  are hardly occupied and  $p(j_+, j_- | i_+, i_-)$  is close to a binary distribution, in which either none or all of the

bound motors in an ensemble perform the power stroke. Only the four states  $(j_+, j_-) = (0, 0)$ ,  $(0, i_-)$ ,  $(i_+, 0)$  and  $(i_+, i_-)$ , which are local minima of  $E$ , can be appreciably occupied. The third part of  $E$  in Eq. (5) decreases by the gain  $E_{pp} < 0$  of conformational energy for each of the  $j_+ + j_-$  *pps* motors. This conformational energy bias is opposed by the first contribution from the elastic energy to  $E$  in Eq. (5) which increases with  $j_{\pm}$ . This elastic energy bias increases with contraction  $z$  (if  $j_{\pm} \geq 1$  and  $z \geq -d$ ) and total spring constant  $K_{\text{tot}}$  and eventually exceeds the conformational bias towards the *pps* state.

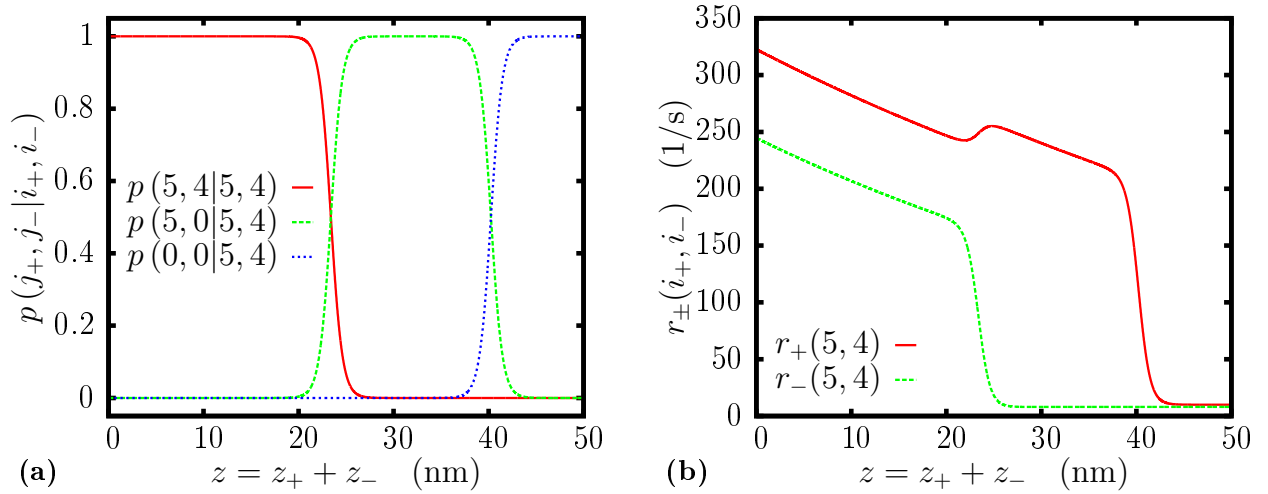


Figure 2. (a) Power-stroke probability  $p(j_+, j_- | i_+, i_-)$  (see Eq. (4)) for a minifilament with  $(i_+, i_-) = (5, 4)$  bound motors as function of contraction  $z = z_+ + z_-$  for external spring stiffness  $K_+ = K_- = 2\text{pNnm}^{-1}$ , that is,  $K_{\text{ext}} = 1\text{pNnm}^{-1}$  and  $K_{\text{tot}} \simeq 0.85\text{pNnm}^{-1}$ . The power-stroke probability is shown for  $(j_+, j_-) = (i_+, i_-)$ ,  $(i_+, 0)$  and  $(0, 0)$ ;  $p(0, i_- | i_+, i_-) = p(0, 4 | 5, 4)$  is smaller than  $10^{-7}$ . (b) Effective reverse rates  $r_+(i_+, i_-)$  and  $r_-(i_+, i_-)$  (see Eq. (8)) as function of  $z$  for the minifilament from (a).

Fig. 2 (a) shows the power-stroke probability  $p(j_+, j_- | i_+, i_-)$  for a minifilament with  $(i_+, i_-) = (5, 4)$  bound motors as function of contraction  $z$ . For small  $z$ , the gain of conformational energy in the power stroke exceeds the increase of elastic energy and the minifilament is in state  $(j_+, j_-) = (i_+, i_-) = (5, 4)$  with probability  $p(i_+, i_- | j_+, j_-) \simeq 1$ . At an intermediate value of  $z$ , the minifilament switches to  $(j_+, j_-) = (i_+, 0) = (5, 0)$  in a sharp transition. This means that above this threshold, only the (+) ensemble with larger number of bound motors ( $i_+ > i_-$ ) is able to perform the power stroke. Above a second threshold, neither ensemble performs the power stroke and the minifilament switches to  $(j_+, j_-) = (0, 0)$ . The plot confirms that the LTE distribution can be almost neglected for intermediate states with  $0 < j_{\pm} < i_{\pm}$  and ensembles are said to

be either in *pps* or *wb* state according to the dominant state of the bound motors.

The thresholds for the transitions can be determined by comparing the energy in the four states with  $j_{\pm} = 0$  or  $j_{\pm} = i_{\pm}$ . For  $i_+ > i_-$  the transition from  $(j_+, j_-) = (i_+, i_-)$  to  $(i_+, 0)$  occurs at  $z \geq -i_- E_{pp}/(K_{\text{tot}}d) - 3d/2$  and from  $(j_+, j_-) = (i_+, 0)$  to  $(0, 0)$  at  $z \geq -i_+ E_{pp}/(K_{\text{tot}}d) - d/2$ . In the symmetric case  $i_+ = i_-$ , the states  $(j_+, j_-) = (i_+, 0)$  and  $(0, i_-)$  are degenerate and the minifilament occupies both with equal probability. It is important to note that the thresholds contain an additional dependence on  $(i_+, i_-)$  via  $K_{\text{tot}}$ . For a given value of  $z$ , fluctuations of  $(i_+, i_-)$  will therefore induce transitions to the *wb* state for small  $i_{\pm}$  and to the *pps* state for large  $i_{\pm}$ .

Fig. 2 (b) plots the effective reverse rates  $r_{\pm}(i_+, i_-)$  in (+) and (-) ensemble as function of  $z$  for the same minifilament setup as in Fig. 2 (a). For small  $z$  the minifilament is in state  $(j_+, j_-) = (i_+, i_-)$  and both rates decrease exponentially with  $z$  due to catch bonding of *pps* motors. Note, however, that the relation between  $z$  and force depends on power-stroke probability: it is  $F_{\text{ext}} = K_{\text{tot}}(z + 2d)$  for  $(j_+, j_-) = (i_+, i_-)$ ,  $F_{\text{ext}} = K_{\text{tot}}(z + d)$  for  $(j_+, j_-) = (i_+, 0)$  and  $F_{\text{ext}} = K_{\text{tot}}z$  for  $(j_+, j_-) = (0, 0)$ . At the transition to  $(j_+, j_-) = (i_+, 0)$ , the bound motors in the (-) ensemble can no longer perform the power stroke and the effective reverse rate of the (-) ensemble drops to the value  $r_-(i_+, 0) \simeq i_- k_{10}$  determined by the small off-rate  $k_{10} \ll k_{20}$  from of the *wb* state. Because the transition to the *wb* state decreases the force on the  $i_+ = 5$  bound motors in the (+) ensemble, the effective reverse rate  $r_+(i_+, 0)$  increases during the transition. With the transition to  $(j_+, j_-) = (0, 0)$  the bound motors in the (+) ensemble enter the *wb* state and the effective reverse rate drops to  $r_+(0, 0) \simeq i_+ k_{10}$ .

## B. Stochastic trajectories

The two dimensional master equation Eq. (9) describes a non-equilibrium process without detailed balance. Moreover, there is a nonlinear feedback between minifilament displacement and binding dynamics so that the master equation cannot be solved analytically. Instead, we analyze minifilament dynamics numerically using the direct method of the Gillespie algorithm. Fig. 3 shows typical stochastic trajectories of symmetric minifilaments with varying size and external spring stiffness. The lower panel of each plot shows the number of bound motors  $(i_+, i_-)$  in the two ensembles. The upper panel plots the minifilament force  $F_{\text{ext}} = F_{\pm}$  from Eq. (2) for a given  $(i_+, i_-)$  weighted with the appropriate conditional probability over  $(j_+, j_-)$ . Due to the

binary nature of the power-stroke probability,  $(j_+, j_-)$  is dominated by the states with  $j_{\pm} = 0$  or  $j_{\pm} = i_{\pm}$ . Fig. 3 (a) shows a trajectory of a small minifilament with  $N_+ = N_- = 4$  motors for  $K_+ = K_- = 0.2\text{pNnm}^{-1}$ , that is,  $K_{\text{ext}} = 0.1\text{pNnm}^{-1}$ . Due to the soft external springs, the power stroke in both ensembles does not increase the load on the motors appreciably so that the effective reverse rate remains close to its large intrinsic value. Moreover, the threshold value of  $z$  for the transition from  $pps$  to  $wb$  state is large and at least one of the ensembles typically detaches before reaching the threshold. Therefore, trajectories are characterized by frequent detachment of ensembles.

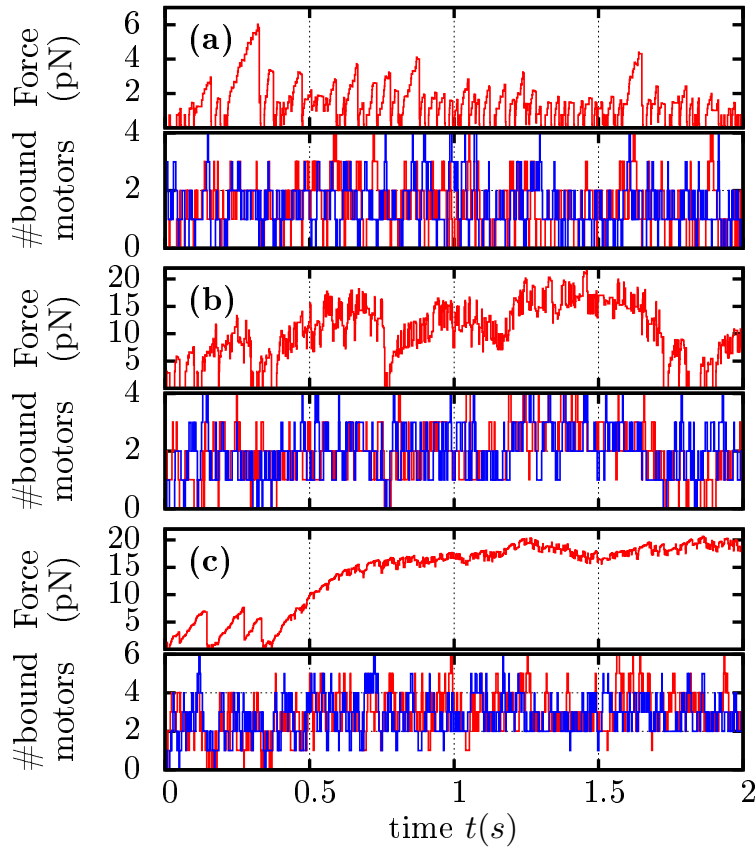


Figure 3. Stochastic trajectories of symmetric minifilaments ( $N_+ = N_-$  and  $K_+ = K_-$ ) with varying ensemble size and varying external spring stiffnesses. In each plot, the bottom panel shows the number of bound motors in (+) ensemble ( $i_+$ , red) and (-) ensemble ( $i_-$ , blue). The top panel shows the force on the ensembles, that is,  $F_{\text{ext}} = F_{\pm}$  (see Eq. (2)) weighted with  $p(j_+, j_- | i_+, i_-)$ . (a)  $N_+ = N_- = 4$  and  $K_+ = K_- = 0.2\text{pNnm}^{-1}$  ( $K_{\text{ext}} = 0.1\text{pNnm}^{-1}$ ), (b)  $N_+ = N_- = 4$  and  $K_+ = K_- = 1.0\text{pNnm}^{-1}$  ( $K_{\text{ext}} = 0.5\text{pNnm}^{-1}$ ) and (c)  $N_+ = N_- = 6$  and  $K_+ = K_- = 0.2\text{pNnm}^{-1}$  ( $K_{\text{ext}} = 0.1\text{pNnm}^{-1}$ ).

Fig. 3 (b) shows a trajectory of a minifilament with the same size as in Fig. 3 (a) but for stiffer external springs with  $K_+ = K_- = 1.0\text{pNnm}^{-1}$  and  $K_{\text{ext}} = 0.5\text{pNnm}^{-1}$ . Detachment is much less frequent than in Fig. 3 (a) and the series of short force peaks is no longer observed. Instead, initial attachment is followed by a gradual increase of force towards a state with strongly fluctuating but on average constant force. This is the result of two effects. First, the force generated by the power stroke at  $z = 0$  decreases the off-rate of *pps* motors appreciably so that the time to detachment of the minifilament is increased. Second, the threshold for the transition from *pps* to *wb* state is lowered and—in combination with smaller off-rate—is more likely to be reached before detachment. To stabilize attachment, it is sufficient that the power stroke cannot be performed for  $i_+ = i_- = 1$  so that the last motor in each ensemble unbinds slowly from the *wb* state. For  $i_+ = i_- = 1$  the transition from  $(j_+, j_-) = (i_+, 0)$  to  $(0, 0)$  occurs at a force  $F_{\text{ext}} \simeq K_{\text{tot}}(z + d) \simeq 9\text{pN}$  below and  $F_{\text{ext}} \simeq K_{\text{tot}}z \simeq 6\text{pN}$  above the transition. The fast fluctuations of force upon binding and unbinding in Fig. 3 (b) thus indicate transitions between *pps* and *wb* state, while the slower variations are due to variations of  $z$  following multiple binding events. Fluctuations to small values of  $z$  allow both ensembles to perform the power stroke and the increased reverse rate can lead to detachment of the minifilament.

Fig. 3 (c) shows a trajectory of a larger minifilament with  $N_+ = N_- = 6$  motors for soft external springs  $K_{\text{ext}} = 0.1\text{pNnm}^{-1}$  as in Fig. 3 (a). Initially, the minifilament detaches repeatedly as observed for the smaller ensemble. Due to its larger size and detachment time, the minifilament eventually reaches the threshold  $F \simeq 7.5 \pm 0.4\text{pN}$  above which the last motors in both ensembles unbind from the *wb* state. Although the minifilament is stalled for  $i_+ = i_- = 1$ , it continues to build up larger force because the typical number of bound motors is larger. For forces above  $F \simeq 16\text{pN}$ , the trajectory of the number of bound motors shows that it becomes unlikely to find a single bound motor. This force is large enough to keep the last two bound motors in the *wb* state with low unbinding rate and to make detachment of any of the two ensembles unlikely.

The dynamics of force can be understood considering the sequence of *pps* to *wb* transitions in Fig. 2. For small  $z$ , both ensembles perform the power stroke and  $z$  increases quickly through the activity of both ensembles. The increase of  $z$  is terminated by the detachment of one of the ensembles. If the minifilament remains attached sufficiently long,  $z$  reaches the threshold above which the ensemble with smaller number of bound motors enters the *wb* state. In this case, the *pps* ensemble moves forward upon binding of motors as long as  $x_{\pm} < 0$ . The *wb* ensemble, on the other hand, will step backward upon binding because  $x_{\pm} > 0$  without *pps* motors. The contraction

$z$  continues to increase as long as the forward movement of the *pps* ensemble is faster than the backward movement of the *wb* ensemble. As  $z$  reaches the threshold above which both ensembles enter the *wb* state,  $z$  can only decrease because  $x_{\pm} > 0$  for  $z > 0$  so that both ensembles step backwards upon binding of motors. Since the threshold is reached first for small  $i_{\pm}$ , detachment of the minifilament becomes very unlikely. On the other hand, for an increasing number of such states the minifilament enters an isometric state in which contraction  $z$  and force  $F_{\text{ext}}$  fluctuate with a constant average, because forward movement at large  $i_{\pm}$  is balanced by backward stepping at small  $i_{\pm}$ .

The trajectories in Fig. 3 are for symmetric minifilaments with the same number  $N_+ = N_-$  of motors in (+) and (-) ensemble and equal external spring constants,  $K_+ = K_-$ . Differences of  $K_+ \neq K_-$  do not affect results, because  $K_{\pm}$  enters the dynamic description only via the effective external spring constant  $K_{\text{ext}}$ . Differences of ensemble sizes,  $N_+ \neq N_-$ , do affect minifilament dynamics but trajectories are qualitatively similar as long as the difference is not too large. Most importantly, asymmetric minifilaments display a net movement in the direction of the larger ensemble. When both ensembles are attached and perform the power stroke, fewer motors are bound on average in the smaller ensemble. These are subject to larger force so that position steps are smaller or even negative; catch bonding of *pps* motors reduces this difference. Moreover, the smaller ensemble detaches more frequently allowing the larger ensemble to move freely. Finally, the smaller ensemble is more likely to transition from *pps* to *wb* state and form a passive anchor for the larger ensemble. The frequency of detachment of asymmetric minifilaments and the probability to reach large forces, though, is determined by the smaller ensemble.

### C. Mechanosensitivity

The stochastic trajectories reveal a switch in minifilament dynamics from transient attachment without sustained force (see Fig. 3 (a)) to near permanent attachment (see Fig. 3 (b-c)) in response to increasing external spring stiffness. To elucidate this mechanosensitivity further, Fig. 4 (a) plots the mean force  $\bar{F}$  obtained by averaging in the steady state generated by symmetric minifilaments with varying ensemble size  $N_+ = N_-$  as function of external spring stiffness  $K_+ = K_- = 2K_{\text{ext}}$ . Fig. 4 (a) reveals a strongly nonlinear increase of  $\bar{F}$  with  $K_{\pm}$ , which is caused by catch bonding of *pps* motors in combination with *pps* to *wb* transitions in the power-stroke probability.

For small stiffness,  $\bar{F}$  increases linearly with  $K_{\pm}$ . Here, the contraction  $z$  reached before one

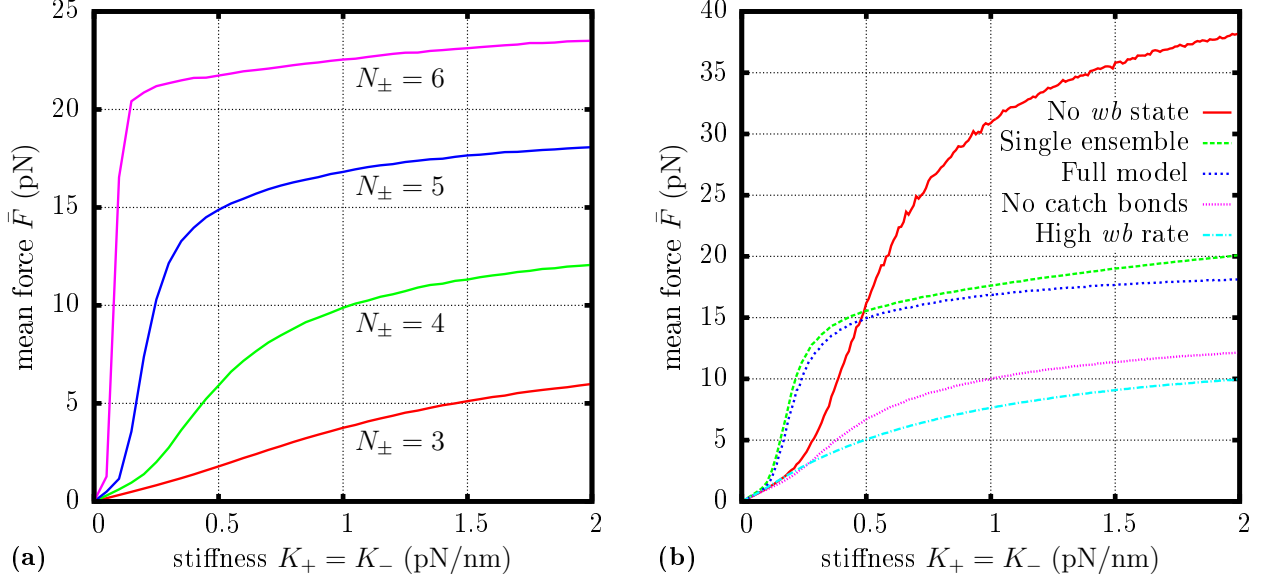


Figure 4. Mean force  $\bar{F}$  generated by symmetric minifilaments with varying number  $N_+ = N_-$  of motors as function of external spring constant  $K_+ = K_- = 2K_{\text{ext}}$ .  $\bar{F}$  is obtained by time averaging over stochastic trajectories. (a) Mean force  $\bar{F}$  for  $N_+ = N_- = 3, 4, 5$  and  $6$ . (b) Mean force  $\bar{F}$  for  $N_+ = N_- = 5$  for several model variants in comparison with the full model: (i) no  $wb$  state, that is, fixed power-stroke probability  $p(i_+, i_- | i_+, i_-) = 1$ , (ii) no catch bonding of  $pps$  motors which unbind with constant off-rate  $k_{20} \simeq 80\text{s}^{-1} = \text{const}$ , (iii) increased off-rate  $k_{10} = 80\text{s}^{-1} = \text{const}$  from the  $wb$  state and (iv) single myosin II ensemble working against an external spring with  $N_+$  and  $K_+$  as for the minifilament.

of the ensembles detaches is on the order of the power-stroke length  $d$ . For small values of  $K_{\text{ext}}$ , the corresponding force is too small to increase the time to detachment significantly, so that the typical contraction  $z$  hardly increases with  $K_{\text{ext}}$ . In the limit of small  $K_{\text{ext}} \ll k_m i_+ i_- / (i_+ + i_-)$ , it is  $K_{\text{tot}} \simeq K_{\text{ext}}$  so that the force  $F_{\text{ext}} = K_{\text{tot}}(z + 2d) \sim K_{\text{ext}}$  is proportional to  $K_{\text{ext}}$ . The mean force along a trajectory is proportional to the duty ratio of a minifilament, that is, the fraction of time both ensembles are attached. The duty ratio is hardly affected by small forces but increases with minifilament size so that the slope in the linear regime increases with  $N_{\pm}$ . Catch bonding of  $pps$  motors eventually increases detachment time and duty ratio so that  $z$  increases beyond the force free case. The mutual positive feedback between force and duty ratio leads to a rapid increase of  $\bar{F}$  which is reinforced by transitions from  $pps$  to  $wb$  state. On the other hand, these transitions limit the increase of force, because  $pps$  motors are required for forward movement of the ensembles and an increase of  $z$ . Once minifilaments are almost permanently

attached,  $\bar{F}$  increases slowly with further increasing  $K_{\pm}$ . This reflects the increase of the average number of bound motors in the isometric state, which is caused by increased force fluctuations for large  $K_{\text{ext}}$  and the nonlinear dependence of the off-rate on force. The increasing number of bound motors allows the minifilament to reach larger values of  $z$  although the  $pps$  to  $wb$  transition occurs for increasing values of  $i_{\pm}$ . The linear regime is most prominent for small  $N_{\pm}$  where the intermediate, super linear regime cannot be discerned. With increasing  $N_{\pm}$ , the linear regime shrinks and the super linear growth in the intermediate regime approaches a step increase of  $\bar{F}$ , because detachment time depends sensitively on changes of the off-rate for large ensembles [37].

Fig. 4 (b) plots the mean force generated by minifilaments with  $N_+ = N_- = 5$  as function of  $K_{\pm}$  for model variants in which components of the myosin II motor cycle are omitted in order to elucidate their contribution to force generation. (i) Without the transition from  $pps$  to  $wb$  state (no  $wb$  state), that is, for fixed power-stroke probability  $p(i_+, i_- | i_+, i_-) = 1$ , the super linear increase of  $\bar{F}$  at intermediate  $K_{\pm}$  is comparable in steepness to the full model but is shifted to larger values of  $K_{\pm}$ . Without stabilization through the  $pps$  to  $wb$  transition, the increase of duty ratio and mean force is due to catch bonding of  $pps$  motors alone. On the other hand,  $\bar{F}$  reaches significantly larger values and continues to increase over the whole range of  $K_{\pm}$  because  $z$  is no longer limited by the transition to the  $wb$  state of both ensembles. Instead,  $\bar{F}$  is limited by the stall force at which the offset  $x_{\pm}$  in both  $pps$  ensembles vanishes. Thus the transition of the power-stroke probability is required to increase the sensitivity of the response and to generate a switch-like behavior with a plateau at large forces. Without this transition, the model would become unphysical because then the power stroke would require more energy than provided by the ATP hydrolysis. (ii) Without catch bonding, that is, with constant off-rate  $k_{20} \simeq 80\text{s}^{-1} = \text{const}$  from the  $pps$  state, the super linear increase of  $\bar{F}$  at intermediate  $K_{\pm}$  is present but occurs for larger  $K_{\pm}$  and is much weaker than in the full model. Also the overall level of  $\bar{F}$  is strongly reduced. Trajectories show that minifilaments do reach the transition from  $pps$  to  $wb$  state, but continue to detach frequently. Thus, catch bonding of  $pps$  motors does not only provide the feedback between force and duty ratio needed for the steep increase of  $\bar{F}$  at intermediate  $K_{\pm}$ , but also stabilizes the isometric state by increasing the average number of bound motors. (iii) With a large off-rate  $k_{10} \simeq 80\text{s}^{-1} = \text{const}$  of  $wb$  motors, transitions from  $pps$  to  $wb$  state increase the effective reverse rates (see Fig. 2). Hence,  $pps$  to  $wb$  transitions induce detachment and neutralize the effect of catch bonding. The level of  $\bar{F}$  is smaller than in the case without catch bonding and a steep intermediate regime is not observed. Thus a low off-rate from the  $wb$  state is required to conserve the large level of force



in the isometric state and to generate the observed switch-like response. (*iv*) A single myosin II ensemble working against an external spring (representing one half of a minifilament), generates slightly larger  $\bar{F}$  than minifilaments because the frequency of detachment is reduced. Due to the larger total spring constant, this difference increases as  $K_{\pm}$  approaches  $k_m$ . For very large  $K_{\pm}$ , on the other hand, the mean force generated by a single ensemble collapses because the power stroke can no longer be performed at  $z = 0$ . This does not occur for minifilaments because  $K_{\text{tot}}$  is limited by  $k_m$ . Thus the interplay between external and internal mechanics is essential for the functioning of minifilaments.

#### D. Ensemble movement on rigid substrates

The contraction  $z$  is confined within a narrow range around a stable fixed point for attached minifilaments. Fluctuations to large  $z$  are limited by the transition of both ensembles to the *wb* state. Fluctuations to small  $z$  induce transitions to the *pps* state in both ensembles so that forward movement of both ensembles increases  $z$  rapidly. The range of  $z$  narrows with increasing  $K_{\text{ext}}$ . To facilitate analysis of this situation, we replace the external springs by rigid anchorage. The total spring constant reduces to  $K_{\text{tot}} = k_m i_+ i_- / (i_+ + i_-)$  and the contraction  $z$  is identical to the sum of the offset  $x_{\pm}$  in the two ensembles,  $z = z_+ + z_- = x_+ + x_-$ . Due to the large stiffness of the neck linkers, at most one ensembles can be in *pps* state at  $z = 0$ , while the other is in *wb* state. The threshold for the transition to state  $(j_+, j_-) = (0, 0)$ , at which the minifilament is stalled, is small and reached within few binding steps. As a consequence a stationary state is established quickly and the time dependent solution  $p_{i_+, i_-}(t)$  of the master equation Eq. (9) can be replaced by the stationary limit  $p_{i_+, i_-}(\infty) = p_{i_+, i_-}(t \rightarrow \infty)$ . Results of stochastic simulations for  $x_{\pm}$  reveal two clearly separated peaks at a negative and a positive value of  $x_+$  (data not shown). The peak at negative  $x_+$  corresponds to the (+) ensemble in *pps* state with force  $k_m(x_+ + d)$  per motor and the peak at positive  $x_+$  to the (+) ensemble in *wb* state with force  $k_m x_+$  per motor. The separation of the peaks equals the power-stroke length,  $d \simeq 8\text{nm}$ , which is the expected difference of  $x_{\pm}$  for  $i_+ = i_-$  (see Eq. (1)). Finite width and asymmetry of the observed peaks are due to fluctuation of  $i_{\pm}$  and  $z$  for the case  $i_+ \neq i_-$ . The same results applies to the offset  $x_-$  in the (-) ensemble.

Stochastic simulations confirm that the ensemble with larger number of bound motors usually performs the power stroke while the other ensemble is in *wb* state (see Fig. 2). For  $i_+ = i_-$ , the minifilament is in state  $(j_+, j_-) = (i_+, 0)$  or  $(0, i_-)$  with equal probability. Therefore, the

power-stroke probability from Eq. (4) can be replaced by

$$p(j_+, j_- | i_+, i_-) = \Theta(i_+ - i_-) \delta_{i_+, j_+} \delta_{0, j_-} + \Theta(i_- - i_+) \delta_{0, j_+} \delta_{i_-, j_-} . \quad (10)$$

where  $\Theta(x)$  is the Heaviside step function with  $\Theta(0) = 1/2$  and  $\delta_{i,j}$  the Kronecker delta. As a consequence of the mechanical coupling of ensembles and the mechanosensitivity of myosin II, the numbers  $i_+$  and  $i_-$  of bound motors in (+) and (-) ensemble are synchronized. The correlation increases with  $N_{\pm}$  but is reduced for minifilaments with soft external springs. Synchronization is due to the transition to the *wb* state of the ensemble with fewer bound motors. The small off-rate of *wb* relative to *pps* motors (see Fig. 2 (b)) tends to equalize the number of bound motors. Soft external springs weaken the mechanical coupling of ensembles so that motors in one ensemble are less sensitive to variations of the number of bound motors in the other. Because minifilaments move in the direction of the *pps* ensemble, synchronization of the number of bound motors tends to reverse the direction of motion of minifilaments and prevents long, persistent runs. This is different from a tug-of-war of processive motors, which are usually described as slip bonds which favor large differences of the number of bound motors.

To derive an approximation for the stationary distribution  $p_{i_+, i_-}(\infty)$  we replace the continuous distribution of  $x_{\pm}$  by a discrete one with two  $\delta$ -peaks. Assuming constant contraction  $z$  during a typical binding and unbinding cycle through states  $(i_+, i_-) = (i + 1, i) \rightarrow (i + 2, i) \rightarrow (i + 2, i + 1) \rightarrow (i + 2, i) \rightarrow (i + 1, i)$  allows to estimate the negative offset in the *pps* ensemble as  $x_{\text{neg}} = -(d/2)(i+1/2)(i+2)^2/(i+1)^3 < 0$ . The offset in the *wb* ensemble is  $x_{\text{neg}} + d > 0$ . For  $i = N_{\pm}/2$ , excellent agreement of this constant strain approximation with stochastic simulations is observed. The load dependent off-rate of *pps* motors becomes independent of  $(i_+, i_-)$ . The strain of *pps* motors in the leading ensemble is  $x_{\text{neg}} + d$  and their off-rate  $\tilde{k}_{20} = k_{20}^0 \exp(-k_m(x_{\text{neg}} + d)/F_0)$ . Together with the binary approximation of Eq. (10) for the power-stroke probability, the off-rate of motors in the (+) ensemble (see Eq. (8)) reduces to

$$r_+(i_+, i_-) = i_+ \left[ \Theta(i_+ - i_-) \tilde{k}_{20} + \Theta(i_- - i_+) k_{10} + (-\tilde{k}_{20} + k_{20}^0) \delta_{i_-, 0} \right] . \quad (11)$$

The first term describes unbinding from the *pps* state, the second from the *wb* state and the third is for vanishing force in the case of a minifilament with detached (-) ensemble. An analogous expression holds for  $r_-(i_+, i_-)$ .

The constant offset approximation yields a two dimensional network of states with constant transition rates per motor. Analytical solutions for the stationary distribution are found by solving

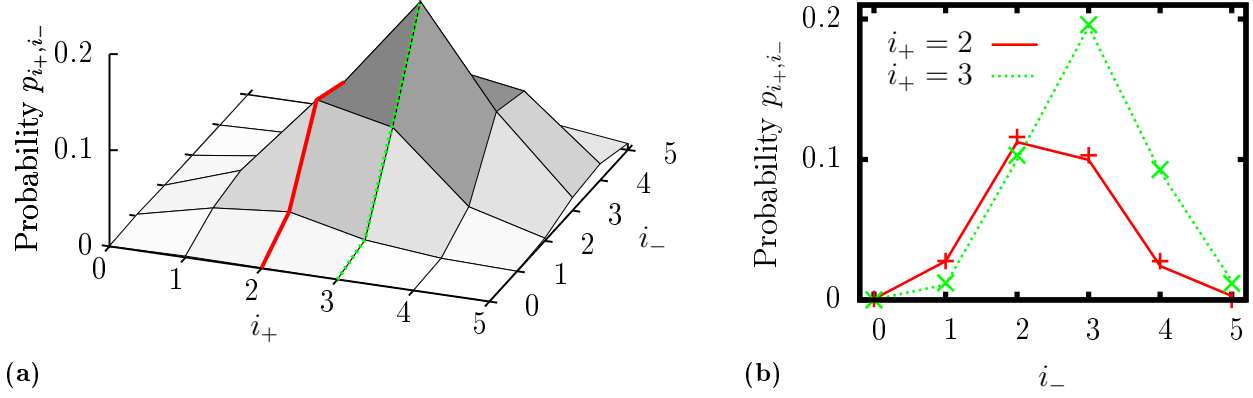


Figure 5. Steady state distribution  $p_{i_+, i_-}(\infty)$  for symmetric minifilaments with  $N_+ = N_- = 5$ . (a) Results of stochastic simulations for  $p_{i_+, i_-}(\infty)$  as function of  $i_+$  and  $i_-$ . Solid and dashed line indicate slices of  $p_{i_+, i_-}(\infty)$  for constant  $i_+ = 2$  and  $i_+ = 3$ . (b) Comparison of simulation results (lines) and analytical results (symbols) from the constant offset approximation for  $p_{i_+, i_-}(\infty)$  as function of  $i_-$  for constant  $i_+ = 2$  and  $i_+ = 3$ .

the corresponding linear system of equations. Fig. 5 (a) shows numerical results for  $p_{i_+, i_-}(\infty)$  from the exact model for a minifilament in a tug-of-war with  $N_+ = N_- = 5$ . The distribution is symmetric with respect to exchanging  $i_+$  and  $i_-$  and strongly peaked at  $i_+ = i_- = 3$ . It is centered along the diagonal with  $i_+ \simeq i_-$  which expresses the effect of synchronization of the ensembles. Fig. 5 (b) shows the stationary probability for fixed  $i_+$  as function of  $i_-$  and compares the numerical solution to the analytical solution obtained via the constant offset approximation. Considering the approximations entering the analytical solution the excellent agreement is quite remarkable.

The absolute position of the minifilament can be defined as the mean position  $z_{\text{abs}} = (z_+ - z_-)/2$  of (+) and (-) ensemble. Symmetric minifilaments perform an unbounded random walk with vanishing mean which is characterized by the diffusion coefficient  $D$ . Due to the limited range of the contraction  $z$ , the diffusion coefficient of  $z_{\text{abs}}$  will be identical to that of  $z_+$  and  $z_-$  in the long time limit,  $D \approx D_+ = D_-$ . We calculate  $D_+$  via the limit of the second jump moment per time in the limit for a vanishing time step as  $2D_+ = d_+$  [41]. For  $i_+ > 0$ , binding in the (+) ensemble yields  $d_+^{\text{bound}} = g_+(i_+) \Delta z_+^2$  where  $\Delta z_+ = -x_+/(i_+ + 1)$ . Detachment of the (+) ensemble releases the strain of both ensembles and yields  $d_+^{\text{detach}} = r_+(i_+, i_-)(x_+ + x_-)^2$  for  $i_+ = 1$ . Movement of the detached (+) ensemble through stepping of the (-) ensemble

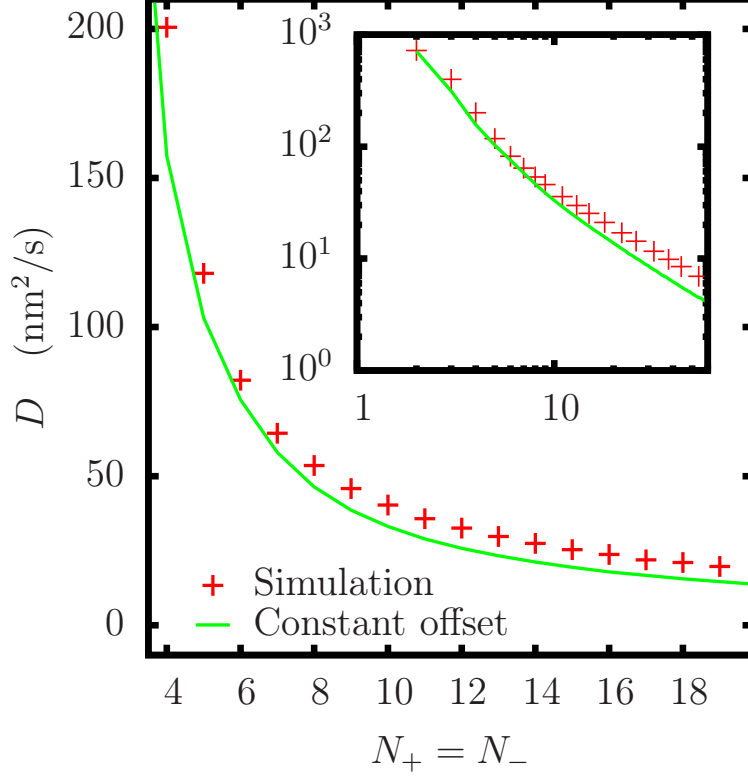


Figure 6. Diffusion constant  $D$  of a minifilament as function of ensemble size  $N_+ = N_-$  for symmetric minifilaments. Numerical results (symbols) are compared to results from the constant strain approximation (see Eq. (12)). The inset shows a logarithmic plot of the data for a wider range of  $N_+$ .

contributes by  $d_+^{\text{drag}} = g_-(i_-)\Delta z_-^2$  for  $i_+ = 0$  and  $i_- > 0$ . The average diffusion constant of the minifilament position  $z_{\text{abs}}$  is

$$D = D_+ = \frac{1}{2} \sum_{i_+=0}^{N_+} \sum_{i_-=0}^{N_-} \left[ d_+^{\text{bound}} + d_+^{\text{detach}} + d_+^{\text{drag}} \right] p_{i_+,i_-}(\infty). \quad (12)$$

Within the constant offset approximation, the offset is  $x_{\text{neg}}$  and  $x_{\text{pos}} = i_-(x_{\text{neg}} + d)/i_+$  when both ensembles are attached and  $-d$  if one of the ensembles is detached. Using the approximate expression for  $p_{i_+,i_-}(\infty)$  from Eq. (10), the contributions to the diffusion constant reduce to

$$d_+^{\text{bound}} = \frac{g_+(i_+)}{(i_+ + 1)^2} \left[ \Theta(i_+ - i_-)x_{\text{neg}}^2 + \Theta(i_- - i_+)x_{\text{pos}}^2 \right] \quad \text{for } i_+ > 0 \quad (13)$$

$$d_+^{\text{detach}} = (x_{\text{neg}} + x_{\text{pos}})^2 \left[ \tilde{k}_{20}\Theta(i_+ - i_-) + k_{10}\Theta(i_- - i_+) \right] \quad \text{for } i_+ = 1 \quad (14)$$

$$d_+^{\text{drag}} = g_-(i_-)\frac{d^2}{(i_- + 1)^2} \quad \text{for } i_+ = 0, i_- > 0. \quad (15)$$

Fig. 6 plots the diffusion constant  $D$  of a minifilament as function of ensemble size  $N_+ = N_-$ . The diffusion coefficient decreases with increasing ensemble size. Simulation results show that for large  $N_{\pm} > 8$ , where detachment of ensembles is negligible, the diffusion coefficient scales as the inverse of ensemble size,  $D \sim N_{\pm}^{-1}$ . For smaller  $N_{\pm}$ , ensemble detachment leads to a stronger dependence on  $N_{\pm}$ . In the approximation of Eq. (12), only  $d_+^{\text{bound}}$  contributes to  $D$  for  $N_{\pm} > 8$ . For a given  $i$ , the squared step  $\Delta z_{\pm}^2$  scales as  $1/(i+1)^2$  and the forward rate as  $N_{\pm} - i$ . Using  $i \simeq N_{\pm}/2$ , this yields the scaling expression  $D \sim (N_{\pm}(1 - 2/N_{\pm}^2))^{-1}$  which fits well to the observed dependence  $D \sim 1/N_{\pm}^{1.12}$ . The deviations between simulation and analytical results are probably due to correlations in the fluctuations of the offset  $x$ . The decrease of  $D$  is in contrast to the dependence of  $D$  on ensemble size in a tug-of-war of processive motors. Processive motors are usually described as slip bonds so that the time to switch between directions increases exponentially with ensembles size, which induces an exponential increase of the diffusion coefficient [42]. The synchronization of the number of bound motors as a consequence of the catch bond character of myosin II leads to a weak dependence of the switching time on ensemble size and prevents the increase of the diffusion coefficient.

#### IV. DISCUSSION AND CONCLUSION

Here we have introduced a new model for the stochastic dynamics of myosin II minifilaments. Analyzing the stochastic trajectories and the mean force generation predicted by our model revealed a switch of the dynamic behavior of the minifilaments in response to changes of the environmental elasticity as a consequence of two independent mechano-sensitive processes. First catch bonding of *pps* motors depends directly on the load on the motors. A gradual increase of load decreases the reverse rate and increases the number of bound motors to stabilize ensemble attachment. Second the transition from *pps* to *wb* state provides another type of catch bonding because unbinding from *wb* state is slower than from *pps* state,  $k_{10} \ll k_{20}$ . There are two important differences: (i) *pps* to *wb* transitions reduce the reverse rates  $r_{\pm}(i_+, i_-)$  abruptly and (ii) the transition is sensitive not only to minifilament load but also to the elasticity of the environment. For single myosin II ensembles, *pps* to *wb* transitions only occur in elastic environments, but not for ensembles working against constant external load [36, 37]. In a minifilament, the elastic neck linkers provide an elastic environment for the ensembles even with rigid anchorage. Therefore our model demonstrates the importance of considering both the internal and external mechanics when

investigating the function of a myosin II minifilament.

Both mechano-sensitive processes cooperate in stabilizing minifilament attachment. While permanent attachment can be reached with catch bonding of *pps* motors alone, the transition from *pps* to *wb* state shifts the switch to smaller external stiffness and steepens the transition. On the other hand, the transition to the *wb* state alone is not sufficient for stable attachment. The two mechano-sensitive processes have contrasting effects on minifilament dynamics. Catch bonding of *pps* motors allows to distribute load on a growing number of bound motors. This increases the velocity of an ensemble at a given load and increases the stall force. In the context of sarcomeric and cytoskeletal myosin II ensembles working against a constant external load, it was shown that catch bonding of *pps* motors leads to the characteristic upward convex force-velocity relation [10, 30, 36, 37]. For minifilaments, catch bonding of *pps* motors increases the mean force exerted in an elastic environment. Transitions from *pps* to *wb* state, on the other hand, limit the increase of force because *pps* motors are required for an increase of contraction, so that minifilaments adjust themselves to an isometric state. In single myosin II ensembles working against a linear external load, the force generated by the ensembles breaks down for very stiff external load because the power stroke can no longer be performed at  $z = 0$ . In minifilaments, the effective stiffness is limited by the elasticity of the neck linkers and this breakdown is prevented. Therefore, minifilaments in the isometric state generate a mean level of force, which depends mainly on the number of motors available for binding, but is robust to variations of elastic properties of the environment. Transitions to the *wb* state limit the mean force as long as they occur before the stall force of an ensemble in *pps* state is reached. This is the case for the parameters in our model; for significantly smaller neck linker stiffness as used in Ref. [35] with comparable power-stroke length, the stall force is reduced strongly and could be reached before the transition to the *wb* state. For the smaller stall force, however, catch bonding of *pps* motors would not be sufficient to decrease the reverse rate sufficiently to achieve stable attachment.

The mechanosensitivity of myosin II minifilaments has important implications for the structure and function of acto-myosin networks. In the actin cortex or reconstituted mixtures of actin with myosin II minifilaments, the apparent stiffness of an actin filament depends largely on the level of crosslinking. Due to their mechanosensitivity, myosin II minifilaments will most efficiently form crosslinks with and exert force to filaments which are already firmly linked to the network. Loose filaments, on the other hand, which do not contribute to overall network tension, could not be integrated by myosin II minifilaments. This could help to create densely linked networks in

which minifilaments provide active crosslinks maintaining a constant level of tension, which is restored after deformations. Stretching a network would initially reinforce attachment and prevent rupture of the network. On longer time scales, the increased tension would be released by the flow of the network as a consequence of backward stepping of minifilaments. Compression, on the other hand, would reduce the load on the minifilament crosslinks. Subsequent forward movement of myosin II ensembles then helps to restore the initial tension in the network. Persistent compression, however, could lead to myosin II detachment and network disintegration. In an actin network of random polarity, mechanosensitivity of myosin II minifilaments in combination with the asymmetric elasticity of actin filaments could lead to a selection of filaments according to their orientation, because large forces can be exerted when filaments are stretched, but small forces on filaments buckling under compression [14, 15]. This could also contribute to the observed contraction rather than expansion of actin networks of random orientation. Unbalanced preferential attachment to strongly linked filaments could cause aggregation of myosin II minifilaments and actin, as it is observed in reconstituted assays [24]. In adherent cells elasticity of the extracellular matrix contributes to the effective stiffness experienced by myosin II minifilaments. Actin stress fibers tend to form and reinforce at focal contacts on sufficiently stiff substrates [16, 43, 44]. Mechanosensitivity of myosin II minifilaments could contribute to discrimination of substrate stiffness because they are not able to crosslink and to build up forces in soft environments. Although this possible relation is rather speculative at this stage and the exact role of myosin minifilaments in the rigidity response of cells is hard to pin down, it is worth mentioning that myosin II activity is an integral part of mechanosensing, which is completely disrupted by inhibiting myosin II activity, e.g. with the pharmacological inhibitor blebbistatin [18].

According to our model, the dynamics of myosin II minifilaments is strongly determined by the existence of at least two load bearing bound states of myosin II motors. For small load, the free energy bias allows the motors to perform the power stroke and complete the motor cycle; for large load, however, the increase of the elastic energy exceeds the free energy bias and the power stroke can no longer be performed. Because the free energy bias is limited by the energy gained in ATP hydrolysis, this transition is inevitable, independent of the parameters. The exact value of the transition thresholds, however, depends on the stiffness  $k_m$  of the neck linkers. This also means that the value of  $k_m$  determines the range of external spring stiffness  $K_{\pm}$  to which minifilaments are sensitive. The values for  $k_m$  used in the literature range over an order of magnitude,  $k_m = 0.3\text{pNnm}^{-1} \dots 3\text{pNnm}^{-1}$  [10, 30, 35, 45]. Although the effect of varying  $k_m$  is reduced

by combining small  $k_m$  with large values of the power-stroke length  $d$ , small values as in Ref. [35] could lead to stalling of minifilaments before the transition of the power-stroke probability is reached. Unless, however, the unbinding force scale  $F_0$  is decreased as well, this stall force would not be enough to achieve stable attachment. Another set of parameters determining the dynamics of myosin II minifilaments in our model are the on- and off-rates of motors, which determine the duty ratio. The load-free duty ratio ( $\rho \simeq 0.33$ ) of myosin II with the transition rates used here is comparable to values reported for non-muscle myosin II isoform B but significantly larger than for non-muscle myosin II isoform A or smooth muscle myosin II. Changes of the transition rates will not change the outcome of the model qualitatively as long as the off-rate from the  $wb$  state is small compared to the off-rate from the  $pps$  state under load. Smaller values of the duty ratio could be compensated by larger ensemble sizes in order to achieve the stabilization of minifilament attachment observed here.

We have further shown with an analytical treatment for the case of minifilaments on rigid substrates that the effective diffusion constant decreases with ensemble size, in marked contrast to the case of the tug-of-war of processive motors, where the diffusion coefficient increases exponentially with the number of motors [42]. Processive motors are usually described as slip bonds favoring strongly asymmetric states, in which one of the ensembles is completely detached. With increasing number of motors, a tug-of-war of processive motors generates persistent movement in either direction, with exceedingly rare reversal of the direction of motion. This dependence of the diffusion coefficient on ensemble size is in line with the function of processive motors for transport, which becomes more efficient with increasing number of motors. Non-processive myosin II motors, on the other hand, serve as active, force generating crosslinks which are not required to move through the cytoskeleton. An experimental realization of a tug-of-war of two ensembles of non-processive motors, e.g. using a solid substrate covered by actin filaments with nematic order but random polarity or bipolar actin constructs on a surface covered with myosin II motors, could be used to investigate the characteristic difference between processive, slip-bond motors and non-processive, catch-bond motors. In general, we envision that biomimetic assays provide rewarding avenues to experimentally test our theoretical predictions.



## ACKNOWLEDGMENTS

The authors acknowledge support by the EU-program MEHTRICS. USS is a member of the Heidelberg cluster of excellence CellNetworks.

---

- [1] J. Howard, *Nature (London)* **389**, 561 (1997).
- [2] M. Schliwa and G. Woehlke, *Nature (London)* **422**, 759 (2003).
- [3] E. L. Holzbaur and Y. E. Goldman, *Current Opinion in Cell Biology* **22**, 4 (2010).
- [4] S. Klumpp and R. Lipowsky, *Proceedings of the National Academy of Sciences of the United States of America* **102**, 17284 (2005).
- [5] G. Koster, M. van Guijn, B. Hofs, and M. Dogterom, *Proceedings of the National Academy of Sciences of the United States of America* **100**, 15583 (2003).
- [6] M. J. I. Müller, S. Klumpp, and R. Lipowsky, *Proceedings of the National Academy of Sciences of the United States of America* **105**, 4609 (2008).
- [7] S. W. Grill, K. Kruse, and F. Jülicher, *Physical Review Letters* **94**, 108104 (2005).
- [8] A. F. Huxley, *Prog. Biophys. Biophys. Chem* **7**, 255 (1957).
- [9] A. F. Huxley and R. M. Simmons, *Nature (London)* **233**, 533 (1971).
- [10] T. A. J. Duke, *Proceedings of the National Academy of Sciences of the United States of America* **96**, 2770 (1999).
- [11] A. Vilfan and T. Duke, *Biophysical Journal* **85**, 818 (2003).
- [12] A. B. Verkhovskiy and G. G. Borisy, *The Journal of Cell Biology* **123**, 637 (1993).
- [13] M. Vicente-Manzanares, X. Ma, R. S. Adelstein, and A. R. Horwitz, *Nature Reviews Molecular Cell Biology* **10**, 778 (2009).
- [14] M. Lenz, T. Thoresen, M. L. Gardel, and A. R. Dinner, *Physical Review Letters* **108**, 238107 (2012).
- [15] M. P. Murrell and M. L. Gardel, *Proceedings of the National Academy of Sciences of the United States of America* **109** pp. 20820 (2012).
- [16] B. Geiger, J. P. Spatz, and A. D. Bershadsky, *Nature Reviews Molecular Cell Biology* **10**, 21 (2009).
- [17] U. S. Schwarz and M. L. Gardel, *J. Cell Sci.* **125**, 3051 (2012).
- [18] D. E. Discher, P. Janmey, and Y.-l. Wang, *Science* **310**, 1139 (2005).
- [19] U. S. Schwarz, T. Erdmann, and I. B. Bischofs, *BioSystems* **83**, 225 (2006).

- [20] J. Solon, I. Levental, K. Sengupta, P. C. Georges, and P. A. Janmey, *Biophysical Journal* **93**, 4453 (2007).
- [21] T. Surrey, F. Nédélec, S. Leibler, and E. Karsenti, *Science* **292**, 1167 (2001).
- [22] D. Mizuno, C. Tardin, C. F. Schmidt, and F. C. MacKintosh, *Science* **315**, 370 (2007).
- [23] P. M. Bendix, G. H. Koenderink, D. Cuvelier, Z. Dogic, B. N. Koeleman, W. M. Briehner, C. M. Field, L. Mahadevan, and D. A. Weitz, *Biophysical Journal* **94**, 3126 (2008).
- [24] M. Soares e Silva, M. Depken, B. Stuhmann, M. Korsten, F. C. MacKintosh, and G. H. Koenderink, *Proceedings of the National Academy of Sciences of the United States of America* **108**, 9408 (2011).
- [25] T. Thoresen, M. Lenz, and M. L. Gardel, *Biophysical Journal* **100**, 2698 (2011).
- [26] T. Thoresen, M. Lenz, and M. L. Gardel, *Biophysical Journal* **104**, 655 (2013).
- [27] E. A. Shah and K. Keren, *eLife* **3**, e01433 (2014).
- [28] S. Leibler and D. A. Huse, *The Journal of Cell Biology* **121**, 1357 (1993).
- [29] A. Vilfan, E. Frey, and F. Schwabl, *Europhysics Letters* **45**, 283 (1999).
- [30] T. Duke, *Philosophical Transactions of the Royal Society of London. Series B: Biological Sciences* **355**, 529 (2000).
- [31] S. Guenther and K. Kruse, *New Journal of Physics* **9**, 417 (2007).
- [32] F. Jülicher, A. Ajdari, and J. Prost, *Reviews of Modern Physics* **69**, 1269 (1997).
- [33] P.-Y. Plaçais, M. Balland, T. Guérin, J.-F. Joanny, and P. Martin, *Physical Review Letters* **103**, 158102 (2009).
- [34] T. Guérin, J. Prost, P. Martin, and J.-F. Joanny, *Current Opinion in Cell Biology* **22**, 14 (2010).
- [35] S. Walcott, D. M. Warshaw, and E. P. Debold, *Biophysical Journal* **103**, 501 (2012).
- [36] T. Erdmann and U. S. Schwarz, *Physical Review Letters* **108**, 188101 (2012).
- [37] T. Erdmann, P. J. Albert, and U. S. Schwarz, *The Journal of Chemical Physics* **139**, 175104 (2013).
- [38] M. Kovács, F. Wang, A. Hu, Y. Zhang, and J. R. Sellers, *Journal of Biological Chemistry* **278**, 38132 (2003).
- [39] S. S. Rosenfeld, J. Xing, L.-Q. Chen, and H. L. Sweeney, *Journal of Biological Chemistry* **278**, 27449 (2003).
- [40] T. Erdmann and U. S. Schwarz, *Physical Review Letters* **92**, 108102 (2004).
- [41] N. van Kampen, *Stochastic Processes in Physics and Chemistry* (North-Holland, 2007), 3rd ed.
- [42] M. J. I. Müller, S. Klumpp, and R. Lipowsky, *Biophysical Journal* **98**, 2610 (2010).
- [43] C.-M. Lo, H.-B. Wang, M. Dembo, and Y.-I. Wang, *Biophysical Journal* **79**, 144 (2000).

[44] B. Geiger and A. D. Bershadsky, *Current Opinion in Cell Biology* **13**, 584 (2001).

[45] B. Chen and H. Gao, *Biophysical Journal* **101**, 396 (2011).